

Article

Metabonomic Analysis of *Macrobrachium rosenbergii* with Iron Prawn Syndrome (IPS)

Xi-Lian Li, Pei-Jing Shen, Wen-Ping Jiang, Ji-Lun Meng, Hai-Hua Cheng and Qiang Gao *

Key Laboratory of Healthy Freshwater Aquaculture, Ministry of Agriculture and Rural Affairs, Key Laboratory of Freshwater Aquaculture Genetic and Breeding of Zhejiang Province, Zhejiang Institute of Freshwater Fisheries, Huzhou 313001, China

* Correspondence: gaoqiang@zjfish.com.cn; Tel.: +86-572-2046227; Fax: +86-572-2045189

Abstract: We previously reported on the comparison of proteomic data between seven tissue types of a novel “iron prawn” species. However, no transcripts or metabolic information are available for this species. We therefore performed shotgun LC–MS/MS metabonomic and RNA-seq analyses of the total protein from “iron prawns”. KEGG analysis revealed that the largest group consisted of a total of 114 KEGG pathway proteins, comparing the “iron prawns” with the normal prawns. A total of 423 peptides, corresponding to metabolic pathways, ABC transporters, starch and sucrose metabolism, insulin resistance/secretion, fatty digestion and absorption, and lipid metabolism, were identified. The pathways of carbohydrate and amino acid metabolism decreased in female iron prawns, while organic acid and its derivatives increased. However, the pathway of organic acid and its derivatives decreased and lipid metabolism increased in the male iron prawns. The pathways of choline metabolism in cancer and glycerophospholipid/histidine/propanoate metabolism have been significantly affected in iron prawns. Our work provides insight into the understanding of the formation mechanism of the “iron prawn”.

Keywords: *Macrobrachium rosenbergii*; metabonomic; transcriptome; LC–MS/MS; iron prawn syndrome



Citation: Li, X.-L.; Shen, P.-J.; Jiang, W.-P.; Meng, J.-L.; Cheng, H.-H.; Gao, Q. Metabonomic Analysis of *Macrobrachium rosenbergii* with Iron Prawn Syndrome (IPS). *Fishes* **2023**, *8*, 196. <https://doi.org/10.3390/fishes8040196>

Academic Editors: Changxu Tian and Zihao Yuan

Received: 20 February 2023

Revised: 29 March 2023

Accepted: 5 April 2023

Published: 9 April 2023



Copyright: © 2023 by the authors. Licensee MDPI, Basel, Switzerland. This article is an open access article distributed under the terms and conditions of the Creative Commons Attribution (CC BY) license (<https://creativecommons.org/licenses/by/4.0/>).

1. Introduction

Iron prawn syndrome (IPS) is a serious disease that endangers the development of *Macrobrachium rosenbergii*, with typical symptoms being sexual precocity and slow growth, resulting in substantial production losses. We previously reported proteomic data on the “iron prawn”; the results showed that the differentially expressed proteins are involved in metabolic processes, namely in muscle contraction, digestive system metabolism, cell differentiation, migration, and apoptosis [1]. Proteomics has only characterized the differentially expressed proteins among different tissues previously; as a technique to a mutually complement genomics, transcriptomics, and proteomics, metabolomics has been used to investigate the metabolic responses to environmental stresses in fish, such as in crucian carps infected by *Edwardsiella tarda* [2], *Perna canaliculus* [3], *Coilia nasus* [4], *Eriocheir sinensis* [5], *Pseudosciaena crocea* [6], *Ctenopharyngodon idellus* [7], *Cynoglossus semilaevis* [8], *Litopenaeus vannamei* [9], *Danio rerio* [10], and *M. rosenbergii* [11], among others.

Gas chromatography–mass spectrometry (GC–MS), liquid chromatography–mass spectrometry (LC–MS) and nuclear magnetic resonance (NMR) are the analytical technologies most frequently used in metabolomics investigations [12,13]. The characteristic beneficial metabolomics in the majority of metabolite structures are not species-specific [14,15]. However, fishes’ metabolic strategy for bacterial infections is largely unknown. In addition, in crustaceans, especially *M. rosenbergii*, researchers aim to identify the underlying pathways through which the animals are exposed to exogenous substances, such as the hepatopancreatic responses to starvation stress [16].

It appears that the differentially expressed metabolites and genes could be responsible for growth retardation in the “iron prawn”, but not for the prolonged molt cycle [17].

However, few studies of the transcriptomics and metabolomics of the “iron prawn” have previously been conducted. To the best of our knowledge, our report is the first to present transcriptomic and metabolomic data for *M. rosenbergii*. In this study, these data were obtained using shotgun LC–MS/MS (two-dimensional liquid chromatography–mass spectrometry) metabolomics strategies and RNA-seq, and the potential pathway and its relative metabolites have been reported. We report on the identification of a wide range of primitive metabolite components and genes, and provide an in-depth description of the transcriptomic and metabolomic data from *M. rosenbergii*.

2. Materials and Methods

2.1. Experimental Sample

This study was approved by Animal Experiment Ethics Committee of Applied Aquatic Genomics Center, Freshwater Fisheries Research Institute of Zhejiang Province. The body weights and lengths of the stunted individuals, obtained from a breeding farm in Gaoyou, Jiangsu Province, were (5.09 ± 0.69) g and (5.27 ± 0.46) cm. Iron and normal prawns (*M. rosenbergii*) both cultured in ponds for 40 days were selected (for the difference, see [1]), and the shrimp were temporarily raised in a 200 L plastic bucket at a temperature of 25 ± 1 °C for a photoperiod cycle of 12 h:12 h. The test water was chlorinated tap water, and pellet feed was supplied daily.

After the shrimp were killed, muscle tissue was collected on ice. In this study, female iron prawn (MA), male iron prawn (MB), female normal prawn (MC) and male normal prawn (MD) were sampled ($n = 6$ per group). Further comparisons (MA vs. MB, MC vs. MA, MC vs. MD, MD vs. MB) have been performed between different genders, normal and iron prawns. All muscle tissues were stored in a freezer at -80 °C until additional processing was conducted. The muscle was ultrasonically dismembered in 1 mL acidified methanol, and the extract was centrifuged (4 °C, $18,000 \times g$, 20 min) to collect the supernatant, which was further processed for metabolomics analysis by shotgun LC–MS/MS. The samples were taken out from the -80 °C freezer and thawed on the ice. To 50 mg of sample, we added 1000 μ L of precooled extractant (70% methanol aqueous solution, containing 1 μ g/mL of 2-chlorophenylalanine as internal standard) as well as precooled steel balls. Homogenization was then conducted for 3 min at 30 Hz. The steel balls were removed before vortexing the solution for 1 min, which was then left to stand on ice for 15 min. Centrifuging was conducted for 10 min, 4 °C, 12,000 r/min, and the supernatant was transferred into the inner liner of an injection bottle for LC–MS/MS analysis.

2.2. Metabonomic Analysis

2.2.1. Total Protein Extraction and Peptide Digestion

The sample was ground into a fine powder, resuspended in a 1:3 ratio of BPP (triphenol protein extraction) solution and swirled at 4 °C for 4 min. Saturated phenol solution, ammonium acetate/methanol solution, pre-cooled acetone, and buffer solution (1% SDS, 8 M urea, protease inhibitor cocktail) were added. The protein concentration was determined using a BCA protein assay kit (Beyotime Biotechnology Co., Shanghai, China) in accordance with the manufacturer’s instructions. The samples were freeze-dried and resuspended in 40 μ L trypsin buffer and incubated at 37 °C for 16–18 h.

2.2.2. Chromatographic Separation and Mass Spectrometry Identification

The mobile phase A was 0.1% formic acid (H_2O) and the mobile phase B was 0.1% formic acid (ACN). For chromatographic separation, a column filled with C18 material (1.8 μ m, 2.1 mm \times 100 mm) from a Waters UPLC column was used. The samples were transferred to a Zorbax 300 sb-c18 peptide trap (Agilent Technologies, Wilmington, DE, USA) and then separated with a chromatographic column. The corresponding liquid gradient was set as 0 to 50 min, and the B-phase gradient was 4–50%. From 50 min to 54 min, the B-phase linear gradient was 50% to 100%. From 54 min to 60 min, the B phase remained at 100%. The hydrolysates were separated by capillary high-performance

liquid chromatography and analyzed using a Q-extraction mass spectrometer (Thermo Fisher Scientific, Waltham, MA, USA). The analysis time was 60 min, and the positive-ion-detection method was used. Mass/charge (m/z) ratios of peptides and peptide fragments were collected according to the following purposes. Some 10 fragment maps (MS2 scan) were obtained after each full scan (m/z 400–1800). Mascot 2.2 software was used to search the Mascot database and obtain the protein identification results. Mascot is a free online search engine, and the following search parameters were used: enzyme digestion, trypsin /P; maximum allowable number of missing sites, 2; fixed modification type, urea methylation (c); variable modification type, oxidation (m); decoy database model, reverse; primary ion mass tolerance, ± 20 ppm; secondary ion mass tolerance, 0.1 Da; and final filtration standard, ≥ 20 .

2.2.3. Non-labeling Quantitation of the Metabonomics

Label-free quantification was used for semi-quantitative analysis of differences in total proteins in any sample and is suitable for semi-quantitative comparison of large sample sizes; instead of metabolites' abundance and concentration, the SWATH technique was used for unlabeled semi-quantitative metabolomics, and significantly different results were obtained in the comparison. Peptide identification was performed using Proteome Discoverer™ (version 2.2, Thermo Scientific) and integrated error discovery rate (FDR) analysis. Search data in the metabolite sequence database were downloaded from UniProt in June 2020 (total: 562,755 entries). The MS/MS spectra were obtained by searching using the following custom search parameters: sample type, identified; cysteine alkylation, MMTS; digestion, trypsin; instrument, Q-Exactive MS; special factors, none; species, none; ID key, biological modification; database, 2020_june_uniprot-zebrafish.fasta; search intensity, thorough; and Roosevelt analysis, yes. Decoy databases were searched using MS/MS spectra to estimate the FDR of peptide identification. The bait database consists of reverse-translated protein sequences from the UniProt Zebrafish database. The FDR analysis was performed on the dataset considering peptides with confidence intervals of $\geq 95\%$.

The data acquisition instrument system mainly uses ultra-performance liquid chromatography (UPLC, shim pack UFLC Shimadzu CBM30A, <https://www.shimadzu.com/>, accessed on 1 January 2020) and tandem mass spectrometry (MS/MS) (QTRAP®, <https://sciex.com/>, accessed on 1 January 2020). Chromatographic column: Waters Acquity UPLC HSS T3 C18 1.8 μm , 2.1 mm \times 100 mm. Mobile phase: phase A is ultra-pure water (0.04% acetic acid) and phase B is acetonitrile (0.04% acetic acid). Elution gradient: 0 min water/acetonitrile (95:5 v/v), 11.0 min 5:95 v/v , 12.0 min 5:95 v/v , 12.1 min 95:5 v/v , 14.0 min 95:5 v/v . Flow rate: 0.4 mL/min. Column temperature: 40 °C. Injection volume: 2 μL . The main mass spectrum conditions were as follows: electrospray ion source (ESI) temperature of 500 °C, mass spectrum voltages of 5500 V (positive) and -4500 V (negative), ion source gas I (GSI) at 55 psi, gas II (GS II) at 60 psi, and curtain gas (cur) at 25 psi; the collision-activated ionization (CAD) parameter was set to extreme. In the triple quadrupole (qtrap), each ion pair was scanned and detected according to the optimized clustering potential (DP) and collision energy (CE) [18].

Based on the self-built targeted standard database MWDB (hardware database), the information and secondary spectrum data were qualitatively analyzed according to the retention time RT (retention time) of the detected substance and the parent and daughter ions. Metabolite quantification was completed by multiple reaction monitoring (MRM) of triple-quadrupole mass spectrometry. In MRM mode, the first quadrupole screens the precursor ions (mother ions) of the target substance and excludes the precursor ions corresponding to other substances to preliminarily eliminate interference; after collision-induced ionization in the second quadrupole, the precursor ions are broken, and a series of distinct fragment ions of the substance are formed according to the structural characteristics of the substance itself. Next, the fragment ions are filtered through the third quadrupole to select a typical characteristic fragment ion. Unless the interference of the target ions is eliminated, the quantification is more accurate, and the repeatability is superior. After

obtaining the data from different samples, the extracted ion chromatographic peaks of all metabolites are integrated under the peak area, and the chromatographic peaks of the same metabolite in different samples are integrated and corrected [19].

2.3. Transcriptomic Analysis, Gene Ontology (GO) and Kyoto Encyclopedia of Genes and Genomes (KEGG) Pathway Annotation

After the qualitative and semi-quantitative analysis of the detected significant different expression genes (DEGs) based on the data from RNA-seq (the parameter, see [4], and the \log_2 fold change and FDR set at ≥ 2 and $\geq 95\%$), we compared the different multiple changes in the semi-quantitative information of DEGs in each group according to the grouping of specific samples. A volcano plot can be used to quickly view the differences in the expression levels of DEGs in two groups of samples, and the statistical significance of these differences. The relationship between different DEGs in each group is displayed in the form of a Venn diagram. By using the GO database, DEGs can be classified by their participation in biological processes (BPs), cellular components (CFs), and molecular functions (MFs). Blast2go software (<http://www.blast2go.com/b2ghome>, accessed on 10 June 2020) was used to transform the identified IDs from the UniProt accession number to GO IDs [4,16]. The GO IDs were submitted to the database for GO annotation. Using the KEGG database, genes can be classified by a participating pathway or function. The UniProt accession of each identified DEG was transformed into the KO ID, according to the ID mapping results of the UniProt database (<http://www.uniprot.org/>, accessed on 1 January 2019). Then, we annotated the DEGs in the KEGG database using the KO ID [4,16].

2.4. The Combined Analysis of Metabonomic and Transcriptomic Data

The combined analysis of metabolites and transcriptomes was performed via redundancy analysis (RDA) [4,7,15]. Integrative techniques are crucial for finding associations between distinct data types and filling mechanistic gaps. The KEGG paths enriched by the two genomics were used to draw bubble maps. Difference multiples for substances with Pearson correlation coefficients greater than 0.80 and p -values less than 0.05 in each difference group are shown by the nine quadrant plots [4,7,15,16]. The results of the correlation calculations for all differentially expressed genes and metabolites are plotted in the correlation-clustering heatmap. Correlations between metabolites and genes are represented by a network, and the results of correlations between differential genes and differential metabolites in each pathway with a Pearson correlation coefficient greater than 0.80 and corrected p -value less than 0.05 are selected for mapping. The O2PLS model was used to perform ensemble analysis between two datasets, including to determine the association between systems bionomics, the association between molecular regulatory mechanisms and phenotypes, and additional intrinsic relationships across a variety of large datasets [4,15]. All differentially expressed genes and metabolites were selected to build the O2PLS model, and variables with strong correlations and weights in different data groups were tentatively judged through load maps to screen out essential variables that influenced alternative omics [4,15].

2.5. Data Analysis

The number of metabolites, that is, the number of hits matched to the database, was expressed as mean \pm standard deviation (SD). Statistically significant differences were determined using a one-way ANOVA and Duncan's multiple range test, with a significance level of $p < 0.05$ [1,4,15,16].

3. Results and Discussion

The mass spectrometry data were processed using Software Analyst 1.6.3, and the results for the mixed QC sample are presented in Figure S1. Based on the local metabolic database, the metabolites in the samples were analyzed qualitatively and semi-quantitatively by mass spectrometry (Table S1). Figure S2a shows the semi-quantitative analysis of inte-

gral correction results for randomly selected metabolites in different samples [20]. The PCA results show the trend of metabolome separation among the groups, indicating whether there were fewer differences in the metabolome between the sample groups (Figure S2b–d), and whether the metabolites were adequately separated (Figure S2e). A total of 423 metabolites were found, as shown in Figure 1a; the results of the highest-ranked metabolites after differential multivariate log 2 processing in the group comparison are shown in Figure 1b. Overall, there were 35 and 34 significantly increased and decreased metabolites, respectively, when comparing between the MA and MC groups (Table 1); the volcano plot is shown in Figure 1c. The MEDN049 (L-saccharopine), MEDN049 (O-phospho-L-serine) and MEDN049 (P-hydroxyphenyl acetic acid) were more abundant in iron prawns, while the MEDN009 (L-aspartic acid), etc., were less abundant (Table 2); the violin chart is shown in Figure S3. The bubble diagram based on the KEGG signaling pathway between the two comparisons is shown in Figure 2. For both genders, vascular smooth muscle contraction, salivary/renin secretion, oxytocin/cGMP-PKG signaling and pathways in cancer, especially choline metabolism, are different. Regarding the differences between the iron and normal prawns, the pathways for histidine metabolism, neuroactive ligand–receptor interactions, and HIF-1 signaling were affected. The shared metabolites and DEGs in the comparisons for the female (with the same health status) gender and iron (with the same gender) were higher than those in the male and normal prawns (Figure 3). The reverse tendency was found in the correlation-clustering heat map (Figure 4), which was supported by the correlation network and the metabolite/DEG-loading diagram presented in Figures 5 and 6. A previous study showed that choline metabolism in cancer and glycerophospholipid metabolism are significantly upregulated in three-year-old fish when compared with five-year-old fish after viral infection [21], which may be related to intestinal trimethylamine N-oxide release [22] and acetylcholinesterase/butyrylcholinesterase [23]. The hypoxia-inducible factor 1 signaling pathway, biosynthesis of amino acids, glycerophospholipid metabolism, and choline metabolism in cancer were enriched, and were found to be notable metabolic pathways that are closely related to temperature shifts in flounder metabolomic and lipidomic analyses [16]. The present study demonstrates that temperature shifts may shape energy metabolism and intestinal health, and alert the HIF-1 signaling pathway; finally, they may result in cancer pathways attributable to iron prawn formation [24].

Table 1. Function annotation and analysis of the “iron prawn” *M. rosenbergii*.

Group Comparison	Total Sig Metabolites	Down-Regulated	Up-Regulated
MC_vs_MA	69	34	35
MD_vs_MB	101	56	45
MA_vs_MB	66	39	27
MC_vs_MD	58	33	25

Table 2. The selected up- and down-regulated metabolites.

Index	Compounds	Type	cpd_ID
MEDN049	L-Saccharopine	up	C00449
MEDN065	O-Phospho-L-Serine	up	C01005
MEDN097	P-Hydroxyphenyl Acetic Acid	up	C00642
MEDN009	L-Aspartic Acid	down	C00049
MEDN011	L-Glutamic Acid	down	C00025
MEDN070	Sarcosine	down	C00213
MEDN082	P-Coumaryl Alcohol	down	C02646
MEDN098	2-Picolinic Acid	down	C10164

Table 2. Cont.

Index	Compounds	Type	cpd_ID
MEDN120	Dulcitol	down	C01697
MEDN200	L-Malic Acid	down	C00149

Note: The method of combining fold change and VIP value of the opls-da model is adopted to screen differential metabolites. Screening criteria: (1) the metabolites with fold change ≥ 2 and fold change ≤ 0.5 were selected. If the difference of metabolites between the control group and the experimental group is more than 2 times or less than 0.5, the difference is considered significant; (2) if there is biological duplication in sample grouping, select metabolites with $VIP \geq 1$ on the basis of the above. The VIP value indicates the influence intensity of the inter-group difference of corresponding metabolites in the classification and discrimination of samples in each group in the model. It is generally considered that the metabolites with $VIP \geq 1$ have significant difference.

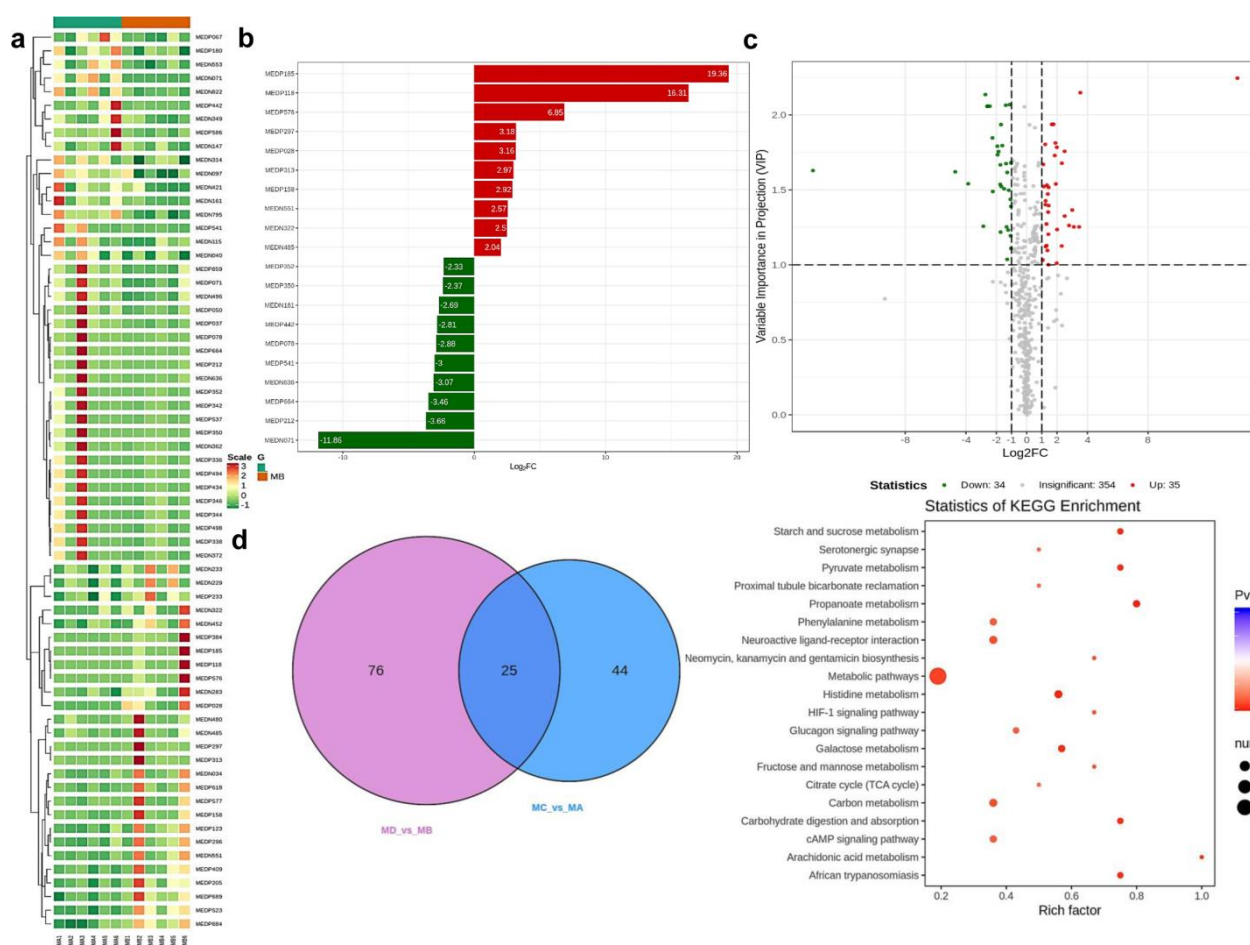


Figure 1. The significant different metabolites in the “iron prawn” *M. rosenbergii*. (a): heatmap analysis was performed on all samples based on normalized data and clustering using R program scripts. (b): metabolite results at the top of the change list. In the (c) volcano plot, abscissa denotes the logarithm of the semi-quantitative difference multiple of a metabolite in the two samples; the ordinate indicates the VIP value. The green dots represent the down-regulated differential expression metabolite, the red dots represent the up-regulated differential expression metabolite, and the dots represent the metabolite detected with negligible differences. (d): Venn diagram for the shared and differing metabolites among the two comparisons (MC vs. MA, MD vs. MB). The richness factor is the ratio of the number of metabolites differentially expressed in the corresponding pathway to the total number of metabolites detected and annotated in the pathway. The larger the value, the greater the enrichment. The closer the *p*-value is to 0, the more significant the enrichment. The size of the points in Figure 1 indicates the number of significantly different metabolites enriched in the corresponding pathway.

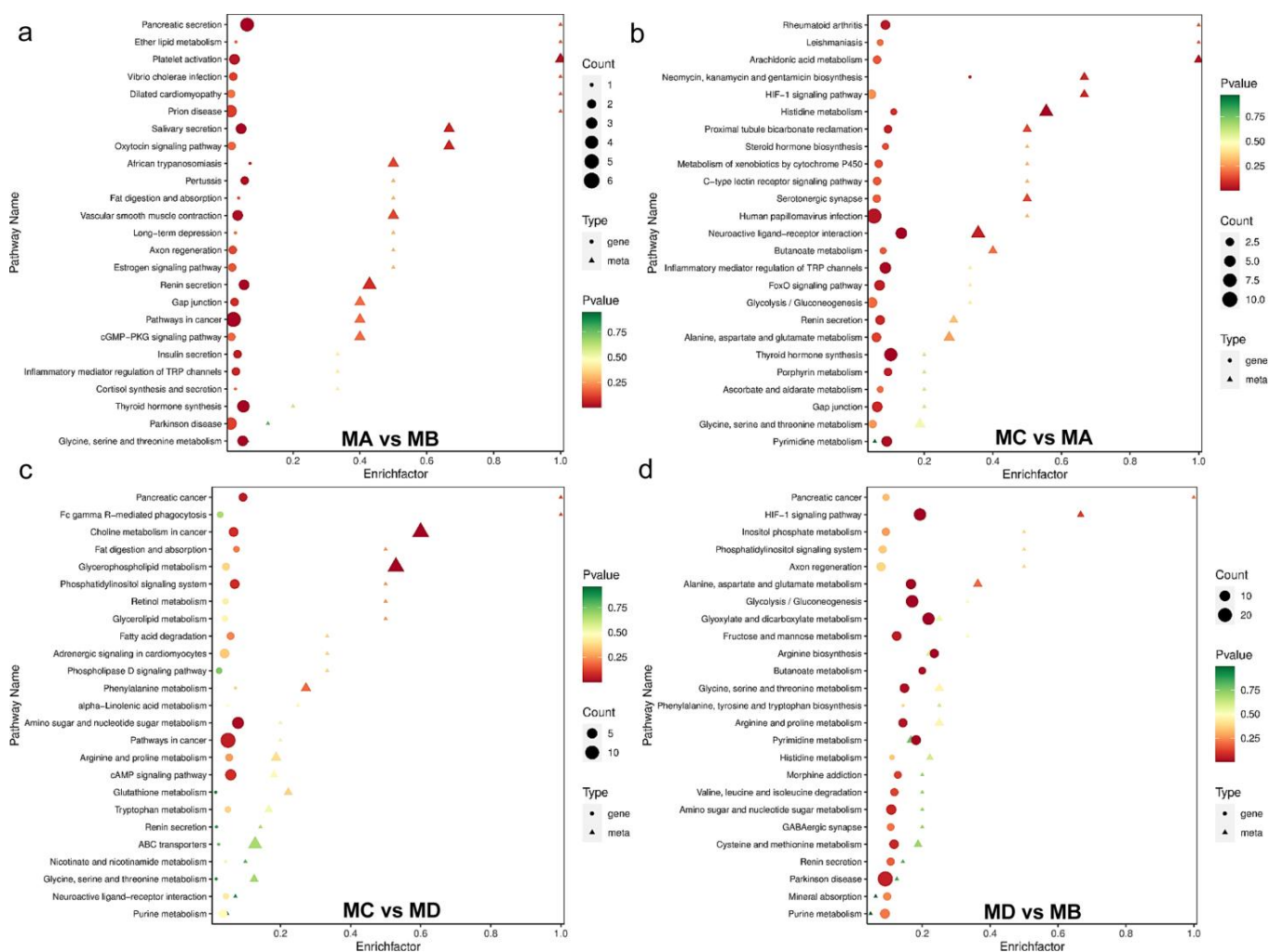


Figure 2. Bubble diagram based on KEGG signaling pathways among the two comparisons of (a) MA vs. MB, (b) MC vs. MA, (c) MC vs. MD, and (d) MD vs. MB. The bubble diagram is a five dimensional diagram, that is, the KEGG path enriched by different assemblages is reflected through horizontal and vertical coordinates, bubble color gradient, shape and size. When the total number of KEGG paths exceeds 25, the transcriptome will prevail, and only the top 25 *p*-value pathways will be displayed. The abscissa represents the enrichment factor (*Diff*/*Background*) of the pathway in different omics, and the ordinate represents the name of the KEGG path; The gradual change of red yellow green represents that the significance of enrichment changes from high to medium to low, expressed by *p*-value; The shape of bubbles represents different genomics, and the size of bubbles represents the number of different metabolites or genes. The larger the number, the larger the point.

The categorized KEGG pathways and the hit numbers (Figure S4) show that metabolic pathways were heavily enriched, as presented in Table 3. A search of the KEGG database revealed that these metabolites are distributed in 114 KEGG pathways. These pathways include metabolic pathways, biosynthesis of secondary metabolites, ABC transporters, glycine, serine and threonine metabolism, biosynthesis of unsaturated fatty acids, carbohydrate digestion and absorption, glucosinolate biosynthesis, fat digestion and absorption, insulin resistance/secretion, protein digestion and absorption, regulation of lipolysis in adipocytes, choline metabolism in cancer, central carbon metabolism in cancer, biosynthesis of amino acids, glycerophospholipid/carbon/ glutathione/ glycerolipid/ glyoxylate and dicarboxylate metabolism, the glucagon/cAMP signaling pathway, glycolysis/ gluconeogenesis, and vitamin digestion and absorption. The most heavily affected KEGG pathways are presented in Table 4, and the shared and specific metabolites between the two comparisons (MC vs. MA,

MD vs. MB) are shown in Figure 1d. The shared and specific metabolite details of the “iron prawn”, *M. rosenbergii* (Table S2), included some metabolites associated with carbohydrate and amino acid metabolism that were decreased in the female iron prawns, while the organic acid and its derivatives increased. Metabolic pathways, ABC transporters, starch and sucrose metabolism, insulin resistance/secretion, fatty digestion and absorption, and lipid metabolism were enriched. These metabolic pathways have been reported in prawns with starvation [16], low pH [25], and salinity [26] stress. The pathways of starch and sucrose metabolism are enriched in *Exopalaemon carinicauda* under thermal stress [27]. The pathways of carbon/lipid/glycerolipid metabolism were reported in ammonia–nitrogen stress [28] and chronic lead exposure [29]. Among them, MEDP174 (purine) has been previously reported in ammonia–N-exposed prawn [28], fish species and other vertebrate animals [30], for example, MEDN201 (succinic Acid) in *Litopenaeus vannamei* [31], and MEDN588 (Glycerol 3-phosphate) in rainbow [32].

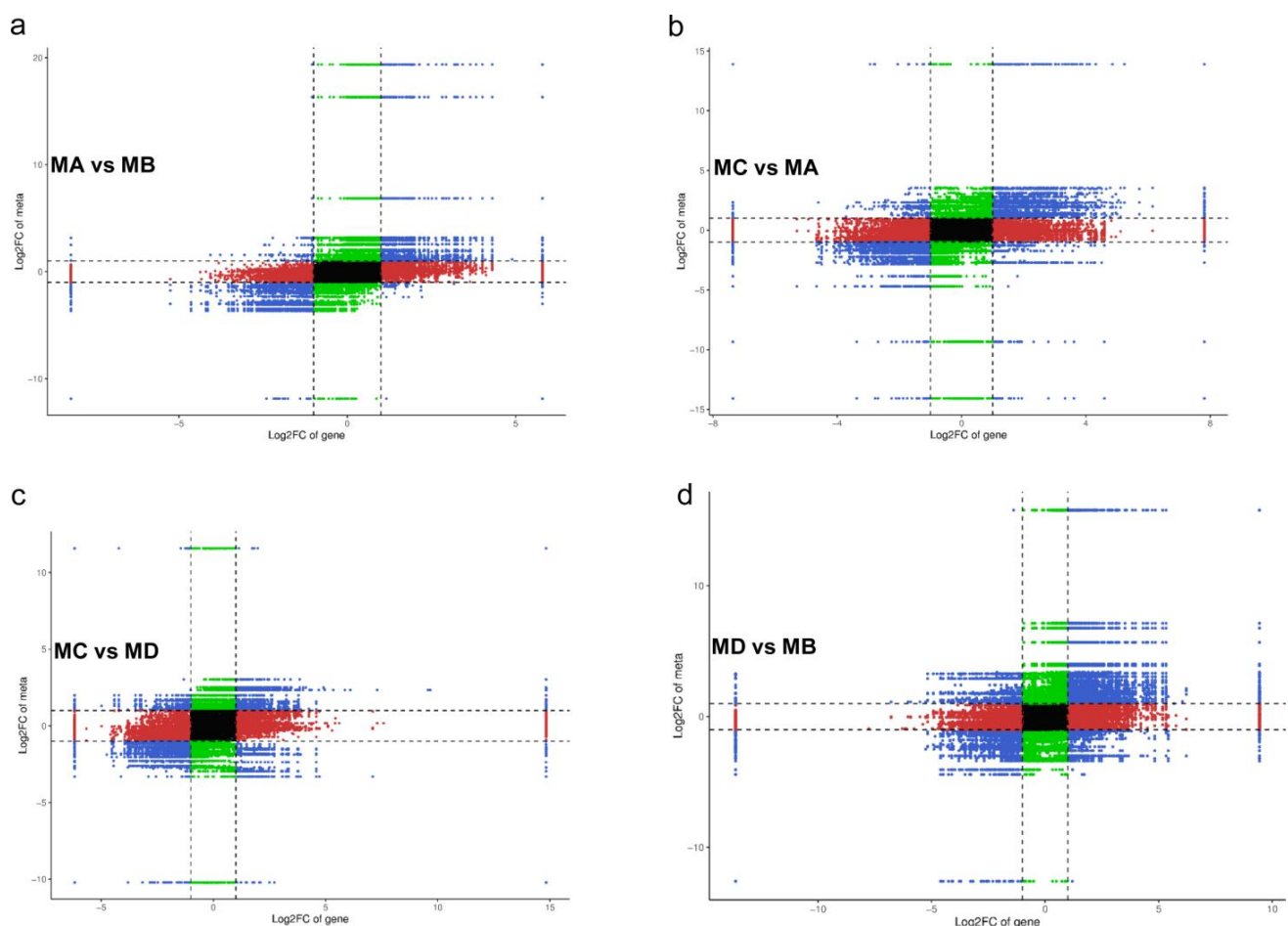


Figure 3. Nine quadrant diagram of correlation analysis of (a) MA vs. MB, (b) MC vs. MA, (c) MC vs. MD, and (d) MD vs. MB). The nine quadrant diagram, which is divided into 1–9 quadrants from left to right and from top to bottom with black dotted line. The abscissa represents \log_2FC of gene, and the ordinate represents \log_2FC of metabolite. Quadrant 5 shows that the differential grouping gene and metabolite are not differentially expressed. Quadrant 3, 7 show that the gene and metabolite are consistent with the differential expression mode of the metabolite. The expression change in the metabolite may be positively regulated by the gene. Quadrant 1,9 shows that contrary to the differential expression pattern of quadrant genes and metabolites, genes and metabolites with inconsistent regulation trends may be negatively regulated by genes. The expression of metabolites in quadrants 2,4, 6, and 8 remains unchanged, the genes are up and down or the gene expression remains unchanged, and the metabolites are up and down.

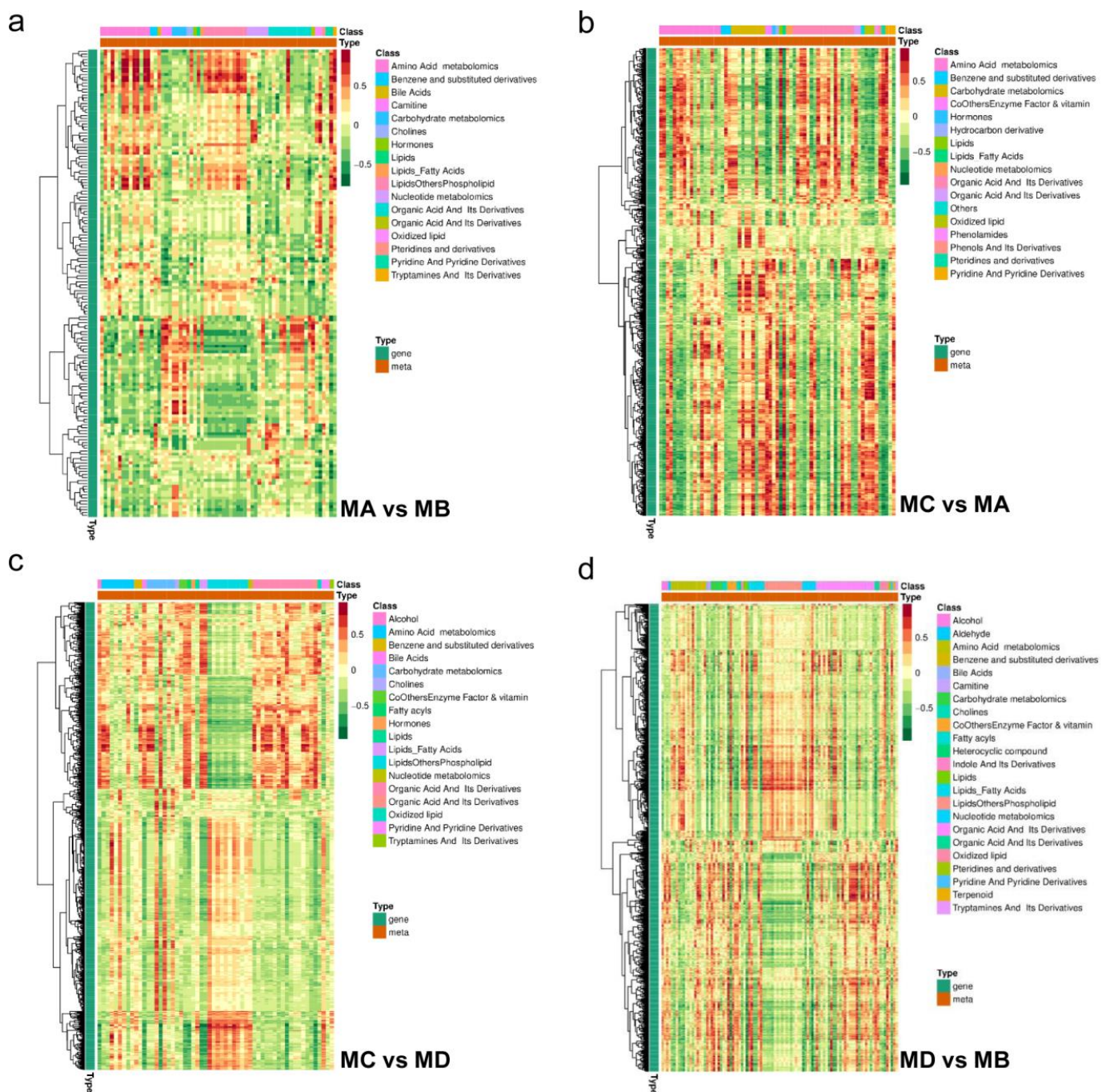


Figure 4. Correlation clustering heat map of (a) MA vs. MB, (b) MC vs. MA, (c) MC vs. MD, and (d) MD vs. MB. Each line in the figure is a gene, and each column is a metabolite. Red represents a positive correlation between genes and metabolites, and green represents a negative correlation between genes and metabolites.

With respect to the male iron prawn, the pathway for organic acids and their derivatives decreased and lipid metabolism increased. The pathways of starch, and sucrose/carbon/galactose metabolism were enriched (Figure 1d). The choline metabolism pathways in cancer and glycerophospholipid/histidine/propanoate metabolism were affected in the iron prawns. A recent study showed self-regulating mechanisms might be the factor preventing prawn from the lethality by obalt-60 gamma radiation, thanks to the existence of the choline metabolism [33]. The glycerophospholipid metabolism has been reported in Jiang et al. [17]; the histidine domain may be related to the activation of caspase-1 [34]. The glycerophospholipid metabolism has

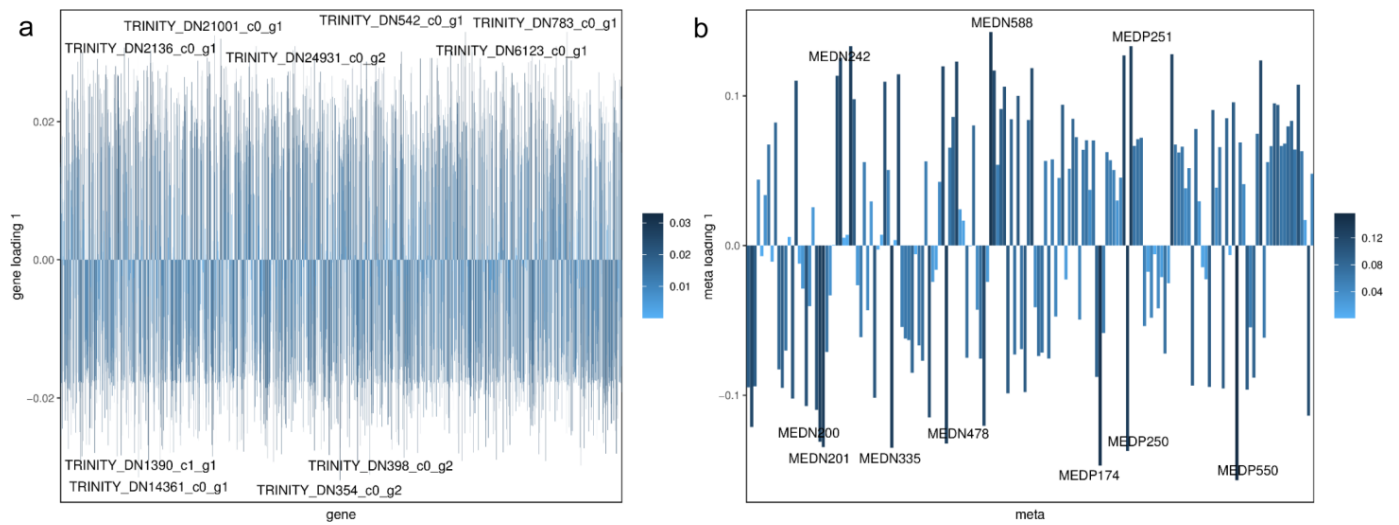


Figure 6. DGEs (a) and Metabolite (b) loadings diagram. The distance from each point to the origin or the height of the histogram in the figure represents the magnitude of the correlation between the substance and another omics, and the darker the color is, the greater the correlation is. The figure shows the top ten substances that have a greater impact on the other omics.

Table 3. The selected pathways among the comparisons.

Comparison Group	Pathway	ko_ID	Unique Compound
MA vs. MB	Metabolic pathways	ko01100	28
	<input type="checkbox"/> Choline metabolism in cancer	ko05231	11
	<input type="checkbox"/> Glycerophospholipid metabolism	ko00564	11
	<input type="checkbox"/> Bile secretion	ko04976	4
	<input type="checkbox"/> Cortisol synthesis and secretion	ko04927	1
	<input type="checkbox"/> Dopaminergic synapse	ko04728	1
	<input type="checkbox"/> Endocrine and other factor-regulated calcium reabsorption	ko04961	1
	<input type="checkbox"/> Endocrine resistance	ko01522	1
	<input type="checkbox"/> Estrogen-signaling pathway	ko04915	1
	<input type="checkbox"/> GnRH-signaling pathway	ko04912	2
	<input type="checkbox"/> Oocyte meiosis	ko04114	1
	<input type="checkbox"/> Ovarian steroidogenesis	ko04913	1
	<input type="checkbox"/> Thyroid hormone-signaling pathway	ko04919	1
	<input type="checkbox"/> Thyroid hormone synthesis	ko04918	1
	<input type="checkbox"/> Vascular smooth muscle contraction	ko04270	2
MC vs. MA	Metabolic pathways	ko01100	37
	<input type="checkbox"/> Biosynthesis of secondary metabolites	ko01110	11
	<input type="checkbox"/> ABC transporters	ko02010	9
	<input type="checkbox"/> Central carbon metabolism in cancer	ko05230	6
	<input type="checkbox"/> Histidine metabolism	ko00340	5
	<input type="checkbox"/> Carbon metabolism	ko01200	5
	<input type="checkbox"/> Neuroactive ligand—receptor interaction	ko04080	5

Table 3. Cont.

Comparison Group	Pathway	ko_ID	Unique Compound
<input type="checkbox"/>	Bile secretion	ko04976	1
<input type="checkbox"/>	Glucagon-signaling pathway	ko04922	3
<input type="checkbox"/>	Glutamatergic synapse	ko04724	1
<input type="checkbox"/>	Glutathione metabolism	ko00480	3
<input type="checkbox"/>	Glycerolipid metabolism	ko00561	1
<input type="checkbox"/>	Glycerophospholipid metabolism	ko00564	1
<input type="checkbox"/>	Glycine, serine and threonine metabolism	ko00260	3
<input type="checkbox"/>	Glycolysis / Gluconeogenesis	ko00010	1
<input type="checkbox"/>	Glyoxylate and dicarboxylate metabolism	ko00630	3
<input type="checkbox"/>	Insulin resistance	ko04931	1
<input type="checkbox"/>	Insulin secretion	ko04911	1
<input type="checkbox"/>	Starch and sucrose metabolism	ko00500	3
<input type="checkbox"/>	Vitamin digestion and absorption	ko04977	1
MC vs. MD	Metabolic pathways	ko01100	21
<input type="checkbox"/>	Glycerophospholipid metabolism	ko00564	9
<input type="checkbox"/>	Choline metabolism in cancer	ko05231	9
<input type="checkbox"/>	ABC transporters	ko02010	6
<input type="checkbox"/>	Biosynthesis of secondary metabolites	ko01110	5
<input type="checkbox"/>	cAMP-signaling pathway	ko04024	2
<input type="checkbox"/>	Fat digestion and absorption	ko04975	1
<input type="checkbox"/>	Fatty acid degradation	ko00071	1
<input type="checkbox"/>	GnRH-signaling pathway	ko04912	1
<input type="checkbox"/>	Regulation of lipolysis in adipocytes	ko04923	1
MD vs. MB	Metabolic pathways	ko01100	35
<input type="checkbox"/>	Biosynthesis of secondary metabolites	ko01110	13
<input type="checkbox"/>	Glycerophospholipid metabolism	ko00564	13
<input type="checkbox"/>	Choline metabolism in cancer	ko05231	13
<input type="checkbox"/>	Central carbon metabolism in cancer	ko05230	6
<input type="checkbox"/>	Biosynthesis of amino acids	ko01230	5
<input type="checkbox"/>	ABC transporters	ko02010	5
<input type="checkbox"/>	Glycine, serine and threonine metabolism	ko00260	4
<input type="checkbox"/>	Biosynthesis of unsaturated fatty acids	ko01040	1
<input type="checkbox"/>	cAMP-signaling pathway	ko04024	4
<input type="checkbox"/>	Carbohydrate digestion and absorption	ko04973	1
<input type="checkbox"/>	Carbon metabolism	ko01200	3
<input type="checkbox"/>	Fat digestion and absorption	ko04975	1
<input type="checkbox"/>	Glucagon-signaling pathway	ko04922	3
<input type="checkbox"/>	Glucosinolate biosynthesis	ko00966	1
<input type="checkbox"/>	Glutathione metabolism	ko00480	2
<input type="checkbox"/>	Glycerolipid metabolism	ko00561	2
<input type="checkbox"/>	Glycolysis / Gluconeogenesis	ko00010	1
<input type="checkbox"/>	Glyoxylate and dicarboxylate metabolism	ko00630	2
<input type="checkbox"/>	Insulin resistance	ko04931	1
<input type="checkbox"/>	Insulin secretion	ko04911	1
<input type="checkbox"/>	Protein digestion and absorption	ko04974	2
<input type="checkbox"/>	Regulation of lipolysis in adipocytes	ko04923	1
<input type="checkbox"/>	Vitamin digestion and absorption	ko04977	2

Table 4. The enriched KEGG pathway among the comparisons.

Comparison Group	Kegg_Pathway	ko_id	Cluter_Frequency	Corrected_p-Value
MA vs. MB	Choline metabolism in cancer	ko05231	11	0.0001
	Glycerophospholipid metabolism	ko00564	11	0.0004
MC vs. MA	Propanoate metabolism	ko00640	4	0.3173
	Histidine metabolism	ko00340	5	0.8170
MC vs. MD	Choline metabolism in cancer	ko05231	9	0.0007
	Glycerophospholipid metabolism	ko00564	9	0.0027
MD vs. MB	Choline metabolism in cancer	ko05231	13	0.0000
	Glycerophospholipid metabolism	ko00564	13	0.0001

4. Conclusions

According to the GO and KEGG analysis results, 423 differentially expressed metabolites and genes were mainly distributed in metabolic pathways, ABC transporters, the starch and sucrose metabolism, insulin resistance/secretion, fat digestion and absorption, and lipid metabolism. Overall, 35 and 34 metabolites were significantly increased and decreased, respectively, in the comparison between the MA and MC groups. Compared with male iron prawns, the representations of the carbohydrate and amino acid metabolism pathways were lower, and organic acids and their derivatives were higher in female iron prawns. The pathways of starch and sucrose/carbon/galactose metabolism were enriched among different genders of normal and iron prawns. The pathways of choline metabolism in cancer, neuroactive ligand–receptor interactions, the HIF-1 signaling pathway and glycerophospholipid/histidine/propanoate metabolism were also distinguished in iron and normal prawns.

Supplementary Materials: The following supporting information can be downloaded at: <https://www.mdpi.com/article/10.3390/fishes8040196/s1>, Figure S1: Superposition diagram of total ion flow diagram (TIC diagram, a) detected by mass spectrometry, MRM metabolite detection multi peak (b) and Tic overlap diagram (c) of the mixed QC sample; Figure S2: The integral correction chart and variability for metabolite semi-quantitative analysis; Figure S3: The data distribution and its probability density via the violin diagram. Figure S4: A metabolite with significant difference, the classification diagram is made according to the types of pathways in KEGG according to the annotation results of KEGG; Table S1: The numbers of the significant expression metabolites and partial calculation results of orthogonal partial least squares discriminant analysis (OPLS-DA) metabolite database mapping table; Table S2: The shared and specific proteins in the detected tissues of the ‘iron prawn’ *M. rosenbergii*.

Author Contributions: X.-L.L. and Q.G. defined the experimental design, managed the experiment, co-wrote the paper, and approved the final draft of the manuscript. P.-J.S., W.-P.J., J.-L.M. and H.-H.C. managed and analyzed the data, prepared figures and/or tables. X.-L.L. performed the statistical analysis. All authors collaborated to interpretation and discussion of the results. All authors have read and agreed to the published version of the manuscript.

Funding: This study was jointly supported by Key Scientific and Technological Grant of Zhejiang for Breeding New Agricultural Varieties (2021C02069-4), Scientific Research Institutes Special Project of Zhejiang Province (2023YSZX002), and Huzhou Special Project for ‘‘Rural Revitalization’’ (2021ZD2036).

Institutional Review Board Statement: The animal study protocol was approved by the Institutional Review Board (or Ethics Committee) of Agriculture Ministry Key Laboratory of Healthy Freshwater Aquaculture (protocol code 2011AA1004020012).

Data Availability Statement: All data generated or analyzed during this study are included in this published article.

Conflicts of Interest: The authors declare no conflict of interest.

References

1. Li, X.L.; Gao, Q.; Shen, P.J.; Zhang, Y.F.; Jiang, W.P.; Huang, Z.Y.; Peng, F.; Gu, Z.M.; Chen, X.F. Proteomic analysis of individual giant freshwater prawn, *Macrobrachium rosenbergii*, growth retardants. *J. Proteom.* **2021**, *241*, 104224. [[CrossRef](#)]
2. Guo, C.; Huang, X.Y.; Yang, M.J.; Wang, S.; Ren, S.T.; Li, H.; Peng, X.X. GC/MS-based metabolomics approach to identify biomarkers differentiating survivals from death in crucian carps infected by *Edwardsiella tarda*. *Fish Shellfish Immunol.* **2014**, *39*, 215–222. [[CrossRef](#)]
3. Young, T.; Alfaro, A.C.; Villas-Bôas, S.G. Metabolic profiling of mussel larvae: Effect of handling and culture conditions. *Aquac. Int.* **2016**, *24*, 843–856. [[CrossRef](#)]
4. Xu, G.; Du, F.; Li, Y.; Nie, Z.; Xu, P. Integrated application of transcriptomics and metabolomics yields insights into population-asynchronous ovary development in *Coilia nasus*. *Sci. Rep.* **2016**, *6*, 31835. [[CrossRef](#)]
5. Ma, Q.; Chen, Q.; Shen, Z.; Li, D.; Han, T.; Qin, J.; Chen, L.; Du, Z. The metabolomics responses of Chinese mitten-hand crab (*Eriocheir sinensis*) to different dietary oils. *Aquaculture* **2017**, *479*, 188–199. [[CrossRef](#)]
6. Liang, P.; Li, R.; Sun, H.; Zhang, M.; Cheng, W.; Chen, L.; Cheng, X.; Akoh, C.C. Phospholipids composition and molecular species of large yellow croaker (*Pseudosciaena crocea*) roe. *Food Chem.* **2018**, *245*, 806–811. [[CrossRef](#)]
7. Zhao, H.; Chong, J.; Tang, R.; Li, L.; Xia, J.; Li, D. Metabolomics investigation of dietary effects on flesh quality in grass carp (*Ctenopharyngodon idellus*). *Gigascience* **2018**, *7*, giy111. [[CrossRef](#)]
8. Jiang, W.; Tian, X.; Fang, Z.; Li, L.; Dong, S.; Li, H.; Zhao, K. Metabolic responses in the gills of tongue sole (*Cynoglossus semilaevis*) exposed to salinity stress using NMR-based metabolomics. *Sci. Total Environ.* **2019**, *653*, 465–474. [[CrossRef](#)] [[PubMed](#)]
9. Liu, F.; Li, S.; Yu, Y.; Sun, M.; Xiang, J.; Li, F. Effects of ammonia stress on the hemocytes of the Pacific white shrimp *Litopenaeus vannamei*. *Chemosphere* **2020**, *239*, 124759. [[CrossRef](#)] [[PubMed](#)]
10. Jiang, Y.X.; Shi, W.J.; Ma, D.D.; Zhang, J.N.; Ying, G.G.; Zhang, H.; Ong, C.N. Dydrogesterone exposure induces zebrafish ovulation but leads to oocytes over-ripening: An integrated histological and metabolomics study. *Environ. Int.* **2019**, *128*, 390–398. [[CrossRef](#)] [[PubMed](#)]
11. Nguyen, T.M.T.; Chen, T.Y.; Shiau, C.Y.; Cheng, Y.T.; Chang, Y.W. Study on biochemical divergences of the meat and egg of freshwater prawns (*Macrobrachium rosenbergii*). *Food Sci. Nutr.* **2019**, *7*, 2017–2023. [[CrossRef](#)] [[PubMed](#)]
12. Kuehnbaum, N.L.; Britz-McKibbin, P. New advances in separation science for metabolomics: Resolving chemical diversity in a post-genomic era. *Chem. Rev.* **2013**, *113*, 2437–2468. [[CrossRef](#)] [[PubMed](#)]
13. Lulijwa, R.; Alfaro, A.C.; Young, T. Metabolomics in salmonid aquaculture research: Applications and future perspectives. *Rev. Aquac.* **2021**, *14*, 547–577. [[CrossRef](#)]
14. Takahashi, H.; Kai, K.; Shinbo, Y.; Tanaka, K.; Ohta, D.; Oshima, T.; Altaf-Ul-Amin, M.; Kurokawa, K.; Ogasawara, N.; Kanaya, S. Metabolomics approach for determining growth-specific metabolites based on Fourier transform ion cyclotron resonance mass spectrometry. *Anal. Bioanal. Chem.* **2008**, *391*, 2769–2782. [[CrossRef](#)] [[PubMed](#)]
15. Rise, M.L.; Martyniuk, C.J.; Chen, M. Comparative physiology and aquaculture: Toward Omics-enabled improvement of aquatic animal health and sustainable production. *Comp. Biochem. Physiol. Part D Genom. Proteom.* **2019**, *31*, 100603. [[CrossRef](#)]
16. Li, F.; Fu, C.; Xie, Y.; Wang, A.; Li, J.; Gao, J.; Cui, X. Transcriptional responses to starvation stress in the hepatopancreas of oriental river prawn *Macrobrachium nipponense*. *Environ. Pollut.* **2019**, *252 Pt A*, 14–20. [[CrossRef](#)]
17. Jiang, Q.; Qian, L.; Gu, S.; Guo, X.; Zhang, X.; Sun, L. Investigation of growth retardation in *Macrobrachium rosenbergii* based on genetic/epigenetic variation and molt performance. *Comp. Biochem. Physiol. Part D: Genom. Proteom.* **2020**, *35*, 100683. [[CrossRef](#)]
18. Chen, W.; Gong, L.; Guo, Z.; Wang, W.; Zhang, H.; Liu, X.; Yu, S.; Xiong, L.; Luo, J. A Novel Integrated method for large-scale detection, identification, and quantification of widely targeted metabolites: Application in the study of rice metabolomics. *Mol. Plant* **2013**, *6*, 1769–1780. [[CrossRef](#)]
19. Fraga, C.G.; Clowers, B.H.; Moore, R.J.; Zink, E.M. Signature-discovery approach for sample matching of a nerve-agent precursor using liquid chromatography-mass spectrometry, XCMS, and chemometrics. *Anal. Chem.* **2010**, *82*, 4165–4173. [[CrossRef](#)]
20. Thévenot, E.A.; Roux, A.; Xu, Y.; Ezan, E.; Junot, C. Analysis of the human adult urinary metabolome variations with age, body mass index, and gender by implementing a comprehensive workflow for univariate and opls statistical analyses. *J. Proteome Res.* **2015**, *14*, 3322–3335. [[CrossRef](#)]
21. He, L.; Zhu, D.; Liang, X.; Li, Y.; Liao, L.; Yang, C.; Huang, R.; Zhu, Z.; Wang, Y. Multi-omics sequencing provides insights into age-dependent susceptibility of grass carp (*Ctenopharyngodon idellus*) to reovirus. *Front. Immunol.* **2021**, *12*, 694965. [[CrossRef](#)]
22. Ebert, T.; Painer, J.; Bergman, P.; Qureshi, A.R.; Giroud, S.; Stalder, G.; Kublickiene, K.; Göritz, F.; Vetter, S.; Bieber, C.; et al. Insights in the regulation of trimethylamine N-oxide production using a comparative biomimetic approach suggest a metabolic switch in hibernating bears. *Sci. Rep.* **2020**, *10*, 20323. [[CrossRef](#)]
23. Akimov, M.G.; Kudryavtsev, D.S.; Kryukova, E.V.; Fomina-Ageeva, E.V.; Zakharov, S.S.; Gretskaia, N.M.; Zinchenko, G.N.; Serkov, I.V.; Makhaeva, G.F.; Boltneva, N.P.; et al. Arachidonoylcholine and other unsaturated long-chain acylcholines are endogenous modulators of the acetylcholine signaling system. *Biomolecules* **2020**, *10*, 283. [[CrossRef](#)]
24. Sun, S.; Xuan, F.; Fu, H.; Ge, X.; Zhu, J.; Qiao, H.; Jin, S.; Zhang, W. Molecular characterization and mRNA expression of hypoxia inducible factor-1 and cognate inhibiting factor in *Macrobrachium nipponense* in response to hypoxia. *Comp. Biochem. Physiol. Part B Biochem. Mol. Biol.* **2016**, *196–197*, 48–56. [[CrossRef](#)]

25. Lu, Z.B.; Li, Y.D.; Jiang, S.G.; Yang, Q.B.; Jiang, S.; Huang, J.H.; Yang, L.S.; Chen, X.; Zhou, F.L. Transcriptome analysis of hepatopancreas in *penaeus monodon* under acute low pH stress. *Fish Shellfish Immunol.* **2022**, *131*, 1166–1172. [[CrossRef](#)] [[PubMed](#)]
26. Fan, Y.; Feng, J.; Xie, N.; Ling, F.; Wang, Z.; Ma, K.; Hua, X.; Li, J. RNA-seq provides novel insights into response to acute salinity stress in oriental river prawn *Macrobrachium nipponense*. *Mar. Biotechnol.* **2022**, *24*, 820–829. [[CrossRef](#)] [[PubMed](#)]
27. Shi, K.; Li, J.; Lv, J.; Liu, P.; Li, J.; Li, S. Full-length transcriptome sequences of ridgetail white prawn *Exopalaemon carinicauda* provide insight into gene expression dynamics during thermal stress. *Sci. Total Environ.* **2020**, *747*, 141238. [[CrossRef](#)] [[PubMed](#)]
28. Dong, X.; Liu, Q.; Kan, D.; Zhao, W.; Guo, H.; Lv, L. Effects of ammonia-N exposure on the growth, metabolizing enzymes, and metabolome of *Macrobrachium rosenbergii*. *Ecotoxicol. Environ. Saf.* **2020**, *189*, 110046. [[CrossRef](#)] [[PubMed](#)]
29. Ding, Z.; Kong, Y.; Shao, X.; Zhang, Y.; Ren, C.; Zhao, X.; Yu, W.; Jiang, T.; Ye, J. Growth, antioxidant capacity, intestinal morphology, and metabolomic responses of juvenile Oriental river prawn (*Macrobrachium nipponense*) to chronic lead exposure. *Chemosphere* **2019**, *217*, 289–297. [[CrossRef](#)]
30. Guasch-Ferré, M.; Bhupathiraju, S.N.; Hu, F.B. Use of metabolomics in improving assessment of dietary intake. *Clin. Chem.* **2018**, *64*, 82–98. [[CrossRef](#)]
31. Duan, Y.; Wang, Y.; Xiong, D.; Zhang, J. RNA-seq revealed the signatures of immunity and metabolism in the *Litopenaeus vannamei* intestine in response to dietary succinate. *Fish Shellfish Immunol.* **2019**, *95*, 16–24. [[CrossRef](#)] [[PubMed](#)]
32. Driedzic, W.R.; Ewart, K.V. Control of glycerol production by rainbow smelt (*Osmerus mordax*) to provide freeze resistance and allow foraging at low winter temperatures. *Comp. Biochem. Physiol. B Biochem. Mol. Biol.* **2004**, *139*, 347–357. [[CrossRef](#)]
33. Stalin, A.; Suganthi, P.; Mathivani, S.; Broos, K.V.; Gokula, V.; Sadiq Bukhari, A.; Syed Mohamed, H.E.; Singhal, R.K.; Venu-Babu, P. Effect of cobalt-60 gamma radiation on total hemocyte content and biochemical parameters in *Macrobrachium rosenbergii* (De Man, 1879). *Int. J. Radiat. Biol.* **2019**, *95*, 753–763. [[CrossRef](#)] [[PubMed](#)]
34. Yuan, H.; Zhang, W.; Jin, S.; Jiang, S.; Xiong, Y.; Chen, T.; Gong, Y.; Qiao, H.; Fu, H. Transcriptome analysis provides novel insights into the immune mechanisms of *Macrobrachium nipponense* during molting. *Fish Shellfish Immunol.* **2022**, *131*, 454–469. [[CrossRef](#)]
35. Lu, X.; Zhang, J.X.; Zhang, L.; Wu, D.; Tian, J.; Yu, L.J.; He, L.; Zhong, S.; Du, H.; Deng, D.F.; et al. Comprehensive understanding the impacts of dietary exposure to polyethylene microplastics on genetically improved farmed tilapia (*Oreochromis niloticus*): Tracking from growth, microbiota, metabolism to gene expressions. *Sci. Total Environ.* **2022**, *841*, 156571. [[CrossRef](#)] [[PubMed](#)]
36. Bouhaddani, S.E.; Houwing-Duistermaat, J.; Salo, P.; Perola, M.; Jongbloed, G.; Uh, H.W. Evaluation of O2PLS in Omics data integration. *BMC Bioinform.* **2016**, *17* (Suppl. S2). [[CrossRef](#)]
37. Fuady, A.M.; El Bouhaddani, S.; Uh, H.W.; Houwing-Duistermaat, J. Estimation of the effect of surrogate multi-omic biomarkers. *Theor. Biol. Forum.* **2021**, *114*, 59–73.

Disclaimer/Publisher’s Note: The statements, opinions and data contained in all publications are solely those of the individual author(s) and contributor(s) and not of MDPI and/or the editor(s). MDPI and/or the editor(s) disclaim responsibility for any injury to people or property resulting from any ideas, methods, instructions or products referred to in the content.